Pergamon

J. Mech. Phys. Solids, Vol. 44, No. 11, pp. 1867–1890, 1996
Copyright © 1996 Elsevier Science Ltd
Printed in Great Britain. All rights reserved
0022–5096/96 $15.00+0.00

PII: S0022–5096(96)00050–6

DYNAMIC COMPRESSIVE FAILURE OF FIBER COMPOSITES

WILLIAM S. SLAUGHTER,† JIANQIANG FAN† and NORMAN A. FLECK‡

† University of Pittsburgh, Mechanical Engineering Department, Pittsburgh, PA 15261, U.S.A. and
‡ Cambridge University Engineering Department, Cambridge CB2 1PZ, U.K.

(*Received* 17 *October* 1995; *in revised form* 18 *March* 1996)

ABSTRACT

A model is presented for the dynamic compressive response of polymer matrix fiber composites. The model includes the effects of fiber misalignment and material nonlinearity as well as material inertia. The role of fiber bending stiffness is included via a couple stress formulation. The response of fiber composites to suddenly applied, constant compressive axial load is examined. It is found that under constant load, inertial effects contribute to a reduction in the critical stress for composite failure. This reduction is greatest for composites with long initial fiber imperfection wavelengths. For a given load, there is a range of initial fiber imperfection wavelengths that will result in composite failure. Within this range, there is a preferred wavelength, which results in the shortest failure time. Copyright © 1996 Elsevier Science Ltd

1. INTRODUCTION

Advanced fiber composites have gained widespread acceptance as structural materials. The benefits of high specific strength and stiffness provided by aligned fiber composites are sufficient to outstrip competing cost considerations in weight critical applications. This is currently most evident in the aerospace industry, but fiber composites are also becoming more common in the automotive and sporting goods industries.

The mechanisms of failure in composite materials are more complex than in monolithic materials. The ability to predict failure accurately for arbitrary loading conditions is important for the efficient design of composite structures, particularly since fiber composites often exhibit little deformation before rupture (Hull, 1981). The complexity of composite failure means, however, that an understanding of uniaxial strength of a unidirectional fiber composite does not translate into an ability to predict strength for general loading of a laminated, multidirectional composite—the mechanisms of failure may be different. In addition, imperfections in the fibers and matrix result in large amounts of scatter in composite strength. An understanding of the mechanisms of failure is required to predict failure reliably. This understanding is also needed for the development of composite materials with greater strength.

The subject of this paper is the dynamic, axial compressive failure of fiber composites. The motivation is the potential use of composites in submersible hulls, which may be subjected to shock loading. Much attention has already been focused

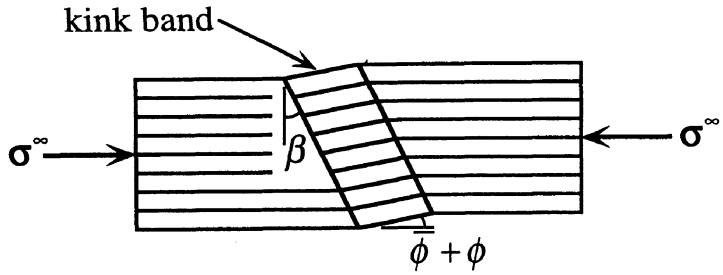

Fig. 1. Schematic diagram of a microbuckle kink band.

on the static compressive failure of fiber composites. The compressive strength of aligned fiber composites is often as low as 60% of the tensile strength. An important mechanism for static compressive failure of polymer matrix materials is plastic microbuckling (Argon, 1972; Budiansky and Fleck, 1993). Microbuckling is a shear instability and occurs by the rotation of fibers within a kink band of width 10–20 fiber diameters (Fig. 1). Typically, the normal to the kink band is inclined at an angle of 15–30°. Microbuckling has also been observed in aluminum alloy composites (Schulte and Minoshima, 1991) and in carbon–carbon composites (Evans and Adler, 1978) and may be a significant failure mechanism in compression–compression fatigue (Huang and Wang, 1989; Slaughter and Fleck, 1993a) and in compressive creep failure (Jelf, 1993; Schapery, 1993; Slaughter and Fleck, 1993; Slaughter *et al.*, 1993).

Argon (1972) has correctly interpreted microbuckling as a plastic collapse phenomenon. He assumed that collapse occurs by the rotation ϕ of fibers which are initially misaligned by a small angle $\bar{\phi}$ within a kink band. The fibers are taken to be inextensible and the composite shear response is assumed to be rigid-perfectly plastic with shear yield stress τ_y. Continuity of traction on the boundary of the kink band implies that the compressive strength σ_c is given by $\sigma_c = \tau_y/\bar{\phi}$. Experimental observations of, for example, Piggott and Harris (1980) and Jelf and Fleck (1992) support the plastic collapse model of microbuckling for polymer matrix composites. Budiansky and Fleck (1993) extended this kinking model of microbuckling to include nonzero kink band angles ($\beta \neq 0$) and plastic strain hardening in the form of a Ramberg–Osgood strain hardening relation. These kinking models neglect the effect of fiber bending stiffness. An alternative couple stress model, which takes fiber bending stiffness into account, has been developed by Fleck *et al.* (1995). In the current paper, the couple stress model is extended to include inertial effects.

The dynamic behavior of fiber composites is not well understood and has only recently begun to be addressed. The lines of inquiry have followed several paths. The dynamic stability of composite structures has been addressed by Shaw *et al.* (1993), Mamalis *et al.* (1994), Bogdanovich and Friedrich (1994) and Gilat and Aboudi (1994). These investigators have analyzed the stability of structures with varying loading conditions and geometries, and examined the role of ply orientation and initial imperfections. The vibration damping characteristics of fiber composites has also been studied (Lesieutre, 1994; Saravanos, 1994; Greif and Hebert, 1995). The passive damping properties of fiber composites have important implications for applications involving flexible structures. The impact and penetration resistance of fiber

composites have obvious ramifications for military applications and have also been investigated (Lagace *et al.*, 1994; Silling and Taylor, 1994).

The objective of this paper is to present a micromechanical model for the dynamic compressive response of an aligned fiber composite. Results are presented for constant axial load. There are no available experimental results for this loading condition, but experimental results for constant strain rates ranging from 10^{-5} to 10^{3} s^{-1} have been obtained for steel reinforced epoxy composites by Sierakowski *et al.* (1971). Jenq and Sheu (1993) have examined the high strain rate behavior of stitched and unstitched glass/epoxy composites. These studies show an increase in dynamic compressive strength over static compressive strength for constant strain rates. They also show that, at moderate strain rates, the mode of failure is analogous to microbuckling in static compressive failure.

2. DYNAMIC COUPLE STRESS MODEL

A micromechanical model is presented for the dynamic compressive response of an axial ply in an aligned fiber composite laminate. The fibers are assumed to have an initial imperfection in the form of a misalignment distribution. The localized nature of the microbuckles that form during compressive failure means that they are in a state of plane strain. The composite is treated as a "smeared-out" continuum—the bending resistance of the fibers is assumed to give rise to couple stresses within the solid. A variation of this model has been used previously for quasi-static deformation (Slaughter and Fleck, 1994; Fleck *et al.*, 1995) and a finite element implementation of the quasi-static couple stress model has been used to examine microbuckle initiation (Fleck and Shu, 1995).

2.1. *Kinematics*

Consider the fiber composite of length L shown in Fig. 2. A coordinate system (x, y) is defined with the coordinate unit vectors $\mathbf{i}$ along the mean fiber direction and $\mathbf{j}$ in the transverse direction. The fibers are assumed to be inextensible and to remain perfectly correlated along the direction $\mathbf{c} = -\sin\beta\mathbf{i} + \cos\beta\mathbf{j}$. Note that the correlation angle β is an input parameter in the analysis and is set to the value of the experimentally

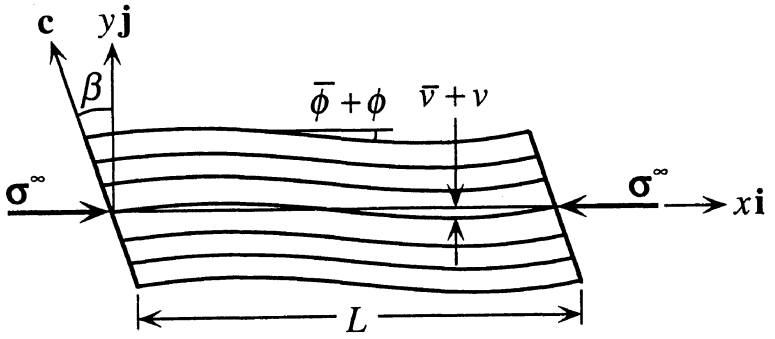

Fig. 2. Schematic diagram of a fiber composite used in the couple stress model.

observed kink band angle formed during microbuckling ($\beta \approx 30°$).† The model is one-dimensional and all field parameters are uniquely expressed as functions of $x+y\tan\beta$. The fiber misalignment distribution is given by the initial angle subtended by the fibers and the mean fiber direction $\bar{\phi}$ $(x+y\tan\beta)$, or equivalently by the initial displacement in the y-direction $\bar{v}$ $(x+y\tan\beta)$. The angle $\bar{\phi}$ and the displacement $\bar{v}$ are related by

$$\bar{\phi} \approx \frac{\partial \bar{v}}{\partial x}, \tag{1}$$

where $\bar{\phi}$ is assumed to be small.

The displacement in the x-direction is negligible since the fibers are treated as inextensible, giving

$$u \approx 0. \tag{2}$$

The fiber rotation ϕ $(x+y\tan\beta)$ is assumed to be small and is related to the displacement in the y-direction v $(x+y\tan\beta)$ by

$$\phi \approx \frac{\partial v}{\partial x}. \tag{3}$$

The components of material acceleration are

$$\begin{aligned} a_x &\approx 0, \\ a_y &= \frac{\partial^2 v}{\partial t^2}, \end{aligned} \tag{4}$$

where t is time. It is convenient to define the state of strain in axes aligned with the local fiber direction. The in-plane components of strain are

$$\begin{aligned} \varepsilon_L &\approx 0, \\ \varepsilon_T &= \frac{\partial v}{\partial y} = \frac{\partial v}{\partial x}\tan\beta, \\ \gamma &\approx \frac{\partial v}{\partial x}, \end{aligned} \tag{5}$$

where ε_L and ε_T are the longitudinal and transverse normal strain components and γ is the engineering shear strain.

† The analysis to follow does not predict the kink band angle. It will transpire that the minimum value of the critical stress for dynamic compressive failure always corresponds to $\beta = 0$, which is not in agreement with experimental observation. It has been suggested (Budiansky, 1983) that the kink band angle is determined by the two-dimensional distribution of initial fiber waviness, which would mean that a one-dimensional model, such as presented here, would be intrinsically unable to predict the kink band angle.

2.2. *Equations of motion*

The stresses acting on an elemental volume of the composite are shown in Fig. 3. These stresses are averaged locally over the fibers and matrix; the length scale of interest in this analysis is large relative to the fiber diameter d and the fiber spacing. σ_L is the normal stress in the fiber direction, σ_T is the transverse normal stress, τ_L is the sliding shear stress in the fiber direction, and τ_T is the transverse shear stress. The fiber bending stiffness gives rise to a couple stress, or moment per unit area, m. The in-plane shear stresses τ_L and τ_T are not, in general, equal. For another example of the use of couple stresses to account for bending stiffness that would otherwise be lost in an homogeneous model of a heterogeneous material, see Biot (1967).

Assuming that the axial stress σ_L is much larger than the other stresses, that the gradient of the axial stress is much larger than the gradient of the sliding shear stress τ_L, and that the gradient of the fiber misalignment angle is small, the equation of motion for the composite in the x-direction is

$$\frac{\partial \sigma_L}{\partial x} \approx 0 \tag{6}$$

and the equation of motion in the y-direction is

$$\frac{\partial \sigma_T}{\partial_y} + \frac{\partial \tau_T}{\partial x} + \sigma_L\left(\frac{\partial^2 \bar{v}}{\partial x^2} + \frac{\partial^2 v}{\partial x^2}\right) \approx \rho \frac{\partial^2 v}{\partial t^2}, \tag{7}$$

where ρ is the density. [These relations follow in a straightforward manner from those given previously by Fleck and Budiansky (1990).] Assuming that angular acceleration is negligible, equilibrium of moments gives the relation between the couple stress and the shear stresses

$$\frac{\partial m}{\partial x} = \tau_L - \tau_T. \tag{8}$$

Equations (6)–(8) can be combined, using the assumption of perfect correlation in the c-direction, to give a single equation of motion

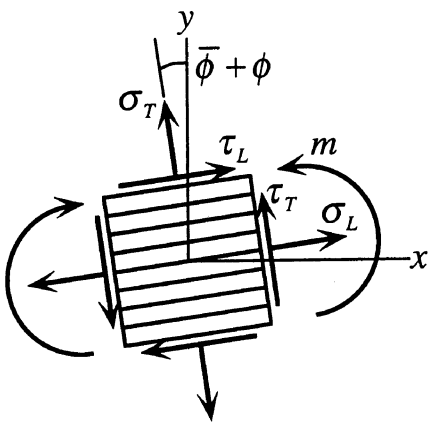

Fig. 3. Composite material element showing the on-axis composite stresses and the composite couple stress.

$$-\frac{\partial^2 m}{\partial x^2}+\sigma_L\left(\frac{\partial^2 \bar{v}}{\partial x^2}+\frac{\partial^2 v}{\partial x^2}\right)+\frac{\partial}{\partial x}(\tau_L+\sigma_T\tan\beta)=\rho\frac{\partial^2 v}{\partial t^2}, \tag{9}$$

where σ_L is independent of x.

2.3. *Constitutive relations*

It is assumed that the fibers behave as linear elastic beams undergoing inextensible bending, and matrix contributions to couple stresses are neglected. Simple beam theory for circular fibers of diameter d, Young's modulus E_f, and volume fraction c_f gives the relation between the couple stress m in the composite and the associated curvature $\partial^2 v/\partial x^2$ as

$$m=\frac{c_f E_f d^2}{16}\frac{\partial^2 v}{\partial x^2}, \tag{10}$$

where $E\equiv c_f E_f$ is interpreted as the approximate elastic modulus of the composite in the fiber direction according to the rule of mixtures, assuming that the fibers are much stiffer than the matrix. The shear and transverse responses of the composite are taken to be those of a nonlinear deformation-theory solid, as suggested by Budiansky and Fleck (1993). They proposed an effective shear stress τ_e defined by

$$\tau_e^2=\tau_L^2+\sigma_T^2/R^2, \tag{11}$$

where the constant R is interpreted as the ratio of yield stresses in transverse tension and in shear. The constitutive relations for the combined stress state were given as†

$$\gamma=\left(\frac{\gamma_e}{\tau_e}\right)\tau_L,$$

$$\varepsilon_T=\left(\frac{\gamma_e}{\tau_e}\right)\frac{\sigma_T}{R^2}, \tag{12}$$

where the effective shear strain γ_e, defined via the virtual work relation $\tau_e\gamma_e=\tau_L\gamma+\sigma_T\varepsilon_T$, is

$$\gamma_e^2=\gamma^2+R^2\varepsilon_T^2. \tag{13}$$

The three parameter (γ_y, τ_y, n) Ramberg–Osgood representation for the in-plane shear stress–strain curve of the composite is taken as the connection

$$\frac{\gamma_e}{\gamma_y}=\frac{\tau_e}{\tau_y}+\frac{3}{7}\left(\frac{\tau_e}{\tau_y}\right)^n \tag{14}$$

between the effective stress and effective strain. Here τ_y is defined as the composite shear yield stress and γ_y is the shear yield strain. Note from (14) that τ_y is the shear stress and $10\gamma_y/7$ is the shear strain at the point on the stress–strain curve where the

† An additional simplifying assumption made in the development of the constitutive relations was that R is also equal to $\sqrt{E_T/G}$, where E_T is the transverse elastic modulus and G is the elastic shear modulus of the composite.

secant modulus is 70% of its initial elastic value $G \equiv \tau_y/\gamma_y$. The strain hardening parameter n ranges from 1 to ∞. For $n > 1$, (14) gives $(d\tau_e/d\gamma_e)_{\gamma_e=0} = \tau_y/\gamma_y = G$. In the limit of $n = 1$, (14) gives the misleading law $\gamma_e = 10/7\ (\tau_e/G)$, and so for $n = 1$, (14) is replaced by the law $\gamma_e = \tau_e/G$; this is referred to as the elastic case.

2.4. *Governing equation*

A governing equation for $v(x, t)$ is obtained by combining the kinematic and constitutive relations with the equation of motion (9). The effective strain (13) is given in terms of displacement v by

$$\gamma_e = \alpha \frac{\partial v}{\partial x}, \tag{15}$$

where $\alpha \equiv \sqrt{1 + R^2 \tan^2 \beta}$. Using (12), (5) and (15), the expression $\tau_L + \sigma_T \tan\beta$ in the equation of motion (9) can be rewritten in terms of the effective stress as

$$\tau_L + \sigma_T \tan\beta = \alpha\tau_e. \tag{16}$$

The equation of motion (9) is then combined with (16) and the constitutive equation for the couple stress (10) to obtain the governing equation

$$-\frac{Ed^2}{16}\frac{\partial^4 v}{\partial x^4} + \sigma_L\left(\frac{\partial^2 \bar{v}}{\partial x^2} + \frac{\partial^2 v}{\partial x^2}\right) + \alpha\frac{\partial \tau_e}{\partial x} = \rho\frac{\partial^2 v}{\partial t^2}, \tag{17}$$

where, from (15) and (14), τ_e is a function of v given by

$$\frac{\alpha}{\gamma_y}\frac{\partial v}{\partial x} = \frac{\tau_e}{\tau_y} + \frac{3}{7}\left(\frac{\tau_e}{\tau_y}\right)^n. \tag{18}$$

For a given initial misalignment distribution $\bar{v}\ (x)$ and axial stress history $\sigma_L(t)$, the governing equation can be solved for the displacement $v(x, t)$.

The governing equation is nondimensionalized through the introduction of the following nondimensional quantities

$$\xi \equiv \frac{x}{l_0}, \quad \tau \equiv \frac{t}{t_0}, \quad s \equiv \frac{\tau_e}{\tau_y}, \quad \Lambda \equiv \frac{-\sigma_L}{G^*}, \quad \Upsilon \equiv \frac{v}{\gamma_y^* l_0}, \quad \bar{\Upsilon} \equiv \frac{\bar{v}}{\gamma_y^* l_0}, \tag{19}$$

where $\gamma_y^* \equiv \gamma_y/\alpha$, $G^* \equiv \alpha^2 G$, and l_0 and t_0 are a characteristic length and time for the composite defined by

$$l_0 \equiv \frac{d}{4}\sqrt{\frac{E}{G^*}}, \quad t_0 \equiv \frac{d\sqrt{\rho E}}{4G^*}. \tag{20}$$

Note that the corresponding characteristic velocity $c_0 = l_0/t_0$ is equal to the transverse elastic wave speed times α. Define also the normalized effective strain

$$\psi \equiv \frac{\gamma_e}{\gamma_y} = \frac{\phi}{\gamma_y^*}, \tag{21}$$

which is related to the nondimensional fiber displacement by

$$\psi = \frac{\partial \Upsilon}{\partial \xi}. \tag{22}$$

Analogously, the normalized initial fiber misalignment angle is

$$\bar{\psi} \equiv \frac{\bar{\phi}}{\gamma_y^*} = \frac{\partial \bar{\Upsilon}}{\partial \xi}. \tag{23}$$

For a typical polymer matrix composite (T800/924C), $d = 8$ μm, $E = 160$ GPa, $E_T = 9.3$ GPa, $G = 6$ GPa, $\sigma_{Ty} = 63$ MPa, $\tau_y = 60$ MPa, $\rho = 1.6 \times 10^3$ kg/m^3, and $\beta = 30^\circ$ (Soutis, 1991). These parameter values correspond to a characteristic length on the order of one fiber diameter, $l_0 = O(d) = 8$ μm, and a characteristic time $t_0 = 4 \times 10^{-9}$ s. The normalized shear modulus and shear yield strain are $G^* = 7.2$ GPa and $\gamma_y^* = 0.0083$.

Now, rewrite the governing equation (17) in terms of the nondimensional quantities (19)

$$\frac{\partial^4 \Upsilon}{\partial \xi^4} + \Lambda\left(\frac{\partial^2 \bar{\Upsilon}}{\partial \xi^2} + \frac{\partial^2 \Upsilon}{\partial \xi^2}\right) + \frac{\partial^2 \Upsilon}{\partial \tau^2} = \frac{\partial s}{\partial \xi}, \tag{24}$$

where the nondimensional effective stress s is a function of the nondimensional fiber displacement Υ as follows. For a Ramberg–Osgood strain hardening material, relation (18) gives

$$\frac{\partial \Upsilon}{\partial \xi} = s\left(1 + \frac{3}{7}|s|^{n-1}\right), \tag{25}$$

while for a linear elastic material

$$\frac{\partial \Upsilon}{\partial \xi} = s. \tag{26}$$

2.5. *Boundary conditions*

Consider a length L of composite subjected to a constant axial stress σ^∞ applied at a time $t > 0$. It is assumed that the ends of the composite have zero applied moment (couple stress m vanishes) and have zero transverse displacement $v = 0$. A variational statement can be constructed for the problem as follows. Consider all displacement fields Υ which satisfy the essential boundary conditions $\Upsilon = 0$ at $\xi = 0$, ξ_L where $\xi_L = \xi(L)$ is the nondimensional length of the composite. Then the governing equation of motion (24) is satisfied when the following functional is rendered stationary with respect to Υ

$$\Pi(\tau) = \int_0^{\xi_L} \left[\frac{1}{2}\left(\frac{\partial^2 \Upsilon}{\partial \xi^2}\right)^2 - \frac{1}{2}\Lambda\left(\frac{\partial \Upsilon}{\partial \xi}\right)^2 + \left(s - \Lambda \frac{\partial \bar{\Upsilon}}{\partial \xi}\right)\frac{\partial \Upsilon}{\partial \xi} + \frac{\partial^2 \Upsilon}{\partial \tau^2}\Upsilon\right] d\xi. \tag{27}$$

Using integration by parts

$$\delta\Pi = \int_0^{\xi_L}\left[\frac{\partial^4\Upsilon}{\partial\xi^4} + \Lambda\left(\frac{\partial^2\bar{\Upsilon}}{\partial\xi^2} + \frac{\partial^2\Upsilon}{\partial\xi^2}\right) + \frac{\partial^2\Upsilon}{\partial\tau^2} - \frac{\partial s}{\partial\xi}\right]\delta\Upsilon\,\mathrm{d}\xi$$
$$+\left[\frac{\partial^2\Upsilon}{\partial\xi^2}\frac{\partial(\delta\Upsilon)}{\partial\xi}\right]\Bigg|_0^{\xi_L} - \left[\frac{\partial^3\Upsilon}{\partial\xi^3} + \Lambda\left(\frac{\partial\bar{\Upsilon}}{\partial\xi} + \frac{\partial\Upsilon}{\partial\xi}\right) - s\right]\delta\Upsilon\Bigg|_0^{\xi_L}. \tag{28}$$

Since $\delta\Upsilon$ is arbitrary, the integrand in (28) vanishes when (24) is satisfied. The last difference relation in (28) vanishes since $\delta\Upsilon = 0$ at $\xi = 0, \xi_L$. The natural boundary condition is

$$\left.\frac{\partial^2\Upsilon}{\partial\xi^2}\right|_{\xi=0,\xi_L} = 0. \tag{29}$$

The boundary condition (29) is a zero moment condition on the ends of the composite. One notes in passing that the last difference relation in (28) results in a zero y-component of traction condition on the ends of the composite, if the ends of the composite are allowed to displace laterally.

The nondimensional parameter Λ can be written as

$$\Lambda = \frac{\sigma^\infty}{G^*}. \tag{30}$$

Λ is the nondimensional compressive axial load applied to the system. In addition, if the load Λ is assumed to be zero until $t = 0$, then the initial conditions are

$$\Upsilon|_{\tau=0} = 0, \tag{31}$$

$$\left.\frac{\partial\Upsilon}{\partial\tau}\right|_{\tau=0} = 0. \tag{32}$$

3. RESULTS

The kinking model of microbuckling (Budiansky and Fleck, 1993) neglects fiber waviness and produces an estimate for the critical load as a function of initial fiber misalignment angle. The static couple stress model (Slaughter and Fleck, 1994; Fleck *et al.*, 1995) presents a more accurate estimate for the critical load by considering the initial fiber misalignment angle distribution. The dynamic couple stress model presented in this paper makes it possible to examine the role inertial effects play in the compressive failure of fiber composites.

In this analysis, it is assumed that the applied load is a step function in time with magnitude σ^∞ for $t > 0$; the dynamic response of fiber composites under constant loading is addressed. Given the nondimensional applied load Λ and the initial fiber waviness, the displacement $\Upsilon(\xi, \tau)$ can be obtained from the solution to the governing equation (24).

It is assumed for simplicity that the initial fiber displacement distribution is sinusoidal,

$$\bar{\Upsilon}(\xi) = \bar{\Upsilon}_m \sin\left(\frac{2\pi\xi}{\lambda}\right), \tag{33}$$

where $\bar{\Upsilon}_m$ is the initial fiber displacement amplitude and λ is the initial wavelength. The corresponding initial fiber misalignment angle distribution is

$$\bar{\psi}(\xi) = \bar{\psi}_m \cos\left(\frac{2\pi\xi}{\lambda}\right), \tag{34}$$

where $\bar{\psi}_m = 2\pi\bar{\Upsilon}_m/\lambda$ is the initial fiber misalignment angle amplitude and is termed the initial imperfection angle. The solution to the governing equation (24) can be expressed as

$$\Upsilon(\xi, \tau) = \chi(\xi, \tau)\bar{\Upsilon}(\xi), \tag{35}$$

where $\chi = \chi(\xi, \tau)$ is the amplification function.

If the initial fiber displacement distribution is periodic, with period λ, and the length of the composite ξ_L is an integer multiple of the wavelength, then by symmetry a solution $\Upsilon(\xi, \tau)$ will exist which is also periodic with period λ. This solution is assumed to be the only solution of interest. Thus, in the analysis to follow, $\xi_L = \lambda$ and the composite length is interpreted as being infinite. Under this assumption, and the misalignment distribution (33), the boundary conditions are satisfied if

$$\Upsilon|_{\xi=0,\xi_L} = 0. \tag{36}$$

3.1. *Elastic solution*

For a linear elastic material with constitutive equation (26), the governing equation reduces to

$$\frac{\partial^4\Upsilon}{\partial\xi^4} + (\Lambda - 1)\frac{\partial^2\Upsilon}{\partial\xi^2} + \frac{\partial^2\Upsilon}{\partial\tau^2} = -\Lambda\frac{\partial^2\bar{\Upsilon}}{\partial\xi^2}. \tag{37}$$

This equation is analogous to that for dynamic elastic buckling of bars (Jones, 1989). The solution to this equation is expressed in the form of (35) where the amplification function is independent of position, i.e. $\chi = \chi(\tau)$; the dependence on time and position are separable in the solution. Substituting (33) and (35) into (37), and dividing by $\bar{\Upsilon}(\xi)$

$$\frac{d^2\chi}{d\tau^2} + [(\omega^2 + 1) - \Lambda]\omega^2\chi = \omega^2\Lambda, \tag{38}$$

where $\omega \equiv 2\pi/\lambda$ is the frequency. The initial conditions (31) and (32) require

$$\chi|_{\tau=0} = 0, \tag{39}$$

$$\left.\frac{d\chi}{d\tau}\right|_{\tau=0} = 0. \tag{40}$$

Solutions to (38) will be bounded if $[(\omega^2 + 1) - \Lambda] > 0$ and unbounded otherwise.

3.1.1. *Critical load.* For a given frequency ω, the dynamic elastic critical load is

$$\Lambda_c^e = 1+\omega^2. \tag{41}$$

If $\Lambda < \Lambda_c^e$, the solution amplification function is

$$\chi(\tau) = \frac{b}{a^2}[1-\cos(a\tau)], \tag{42}$$

where

$$a^2 = \omega^2[(\omega^2+1)-\Lambda],$$
$$b = \Lambda\omega^2. \tag{43}$$

The amplification function oscillates in time, but remains bounded. This is demonstrated in Fig. 4, where the frequency $\omega = 1$, corresponding to a critical load $\Lambda_c^e = 2$. As the load approaches the critical load, both the amplitude and wavelength of oscillation increase. The mean value of $\chi(\tau)$, about which oscillation occurs, is the solution for static loading.

If $\Lambda > \Lambda_c^e$, the solution amplification function is

$$\chi(\tau) = \frac{b}{a^2}[\cosh(a\tau)-1], \tag{44}$$

where

$$a^2 = \omega^2[\Lambda-(\omega^2+1)],$$
$$b = \Lambda\omega^2. \tag{45}$$

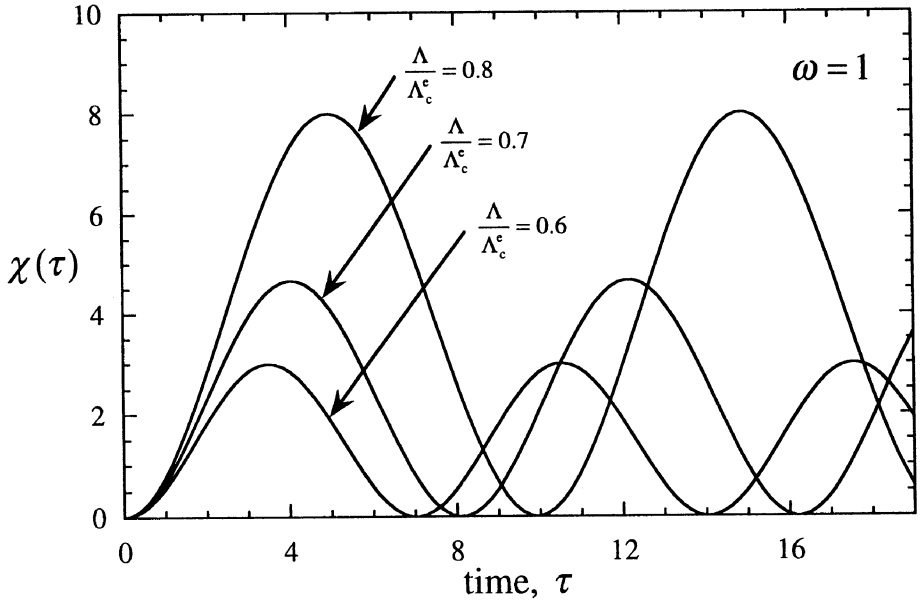

Fig. 4. Amplification function for a linear elastic constitutive relation and for loads less than the critical load.

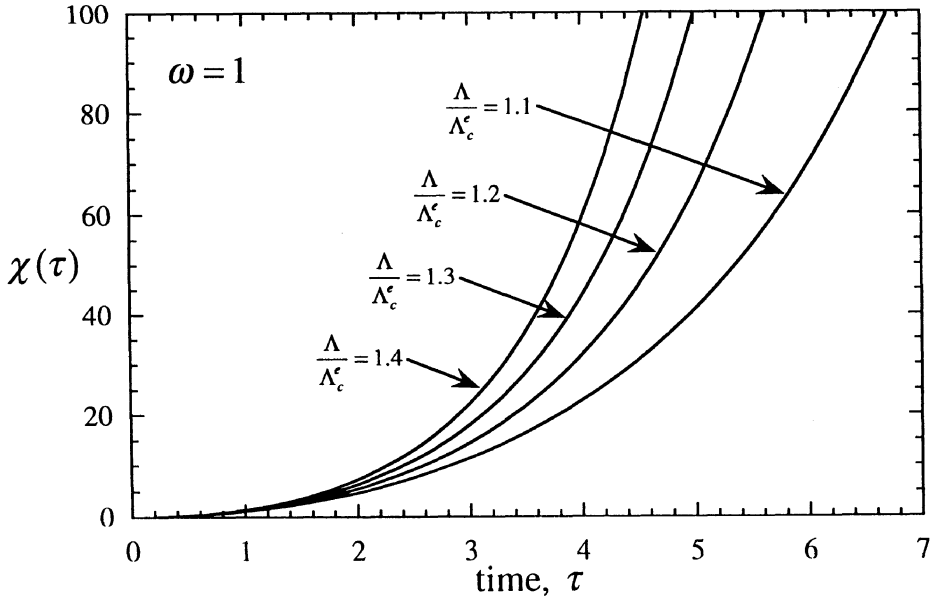

Fig. 5. Amplification function for a linear elastic constitutive relation and for loads greater than the critical load.

The amplification function is unbounded, increasing exponentially as time progresses, as shown in Fig. 5. Therefore, Λ_c^e can be reasonably defined as a critical load or buckling load. This critical load is a measure of the dynamic compressive strength of linear elastic fiber composites under constant loading. If $\Lambda \geqslant \Lambda_c^e$, the fiber composite is unstable, and the composite will fail; if $\Lambda < \Lambda_c^e$, the fiber composite remains stable.

Note that the dynamic elastic buckling load Λ_c^e is independent of the initial misalignment amplitude. In the limit as the initial misalignment wavelength approaches infinity, the dynamic elastic buckling load approaches unity

$$\lim_{\lambda \to \infty} \Lambda_c^e = 1. \tag{46}$$

This is the static elastic buckling load predicted by Rosen (1965) and Budiansky and Fleck (1993) using static analysis: the dynamic elastic buckling load is the same as the static elastic buckling load when the wavelength approaches infinity.

3.1.2. *Critical frequency*. For a given load Λ, initial imperfections with frequencies greater than the dynamic elastic critical frequency

$$\omega_c^e = \sqrt{\Lambda - 1} \tag{47}$$

will give rise to an amplification function (42), which oscillates stably in time. For frequencies less than ω_c^e, the amplification function (44) blows up exponentially. This is shown in a plot of amplification function $\chi(\omega, \tau)$ versus frequency ω for different values of time τ at a load $\Lambda = 2$ (Fig. 6). The amplification functions for frequencies $\omega > \omega_c^e$ are bounded in time while for $\omega < \omega_c^e$ they increase monotonically.

The rate at which $\chi(\omega, \tau)$ increases for $\omega < \omega_c^e$ is not uniform; some frequencies

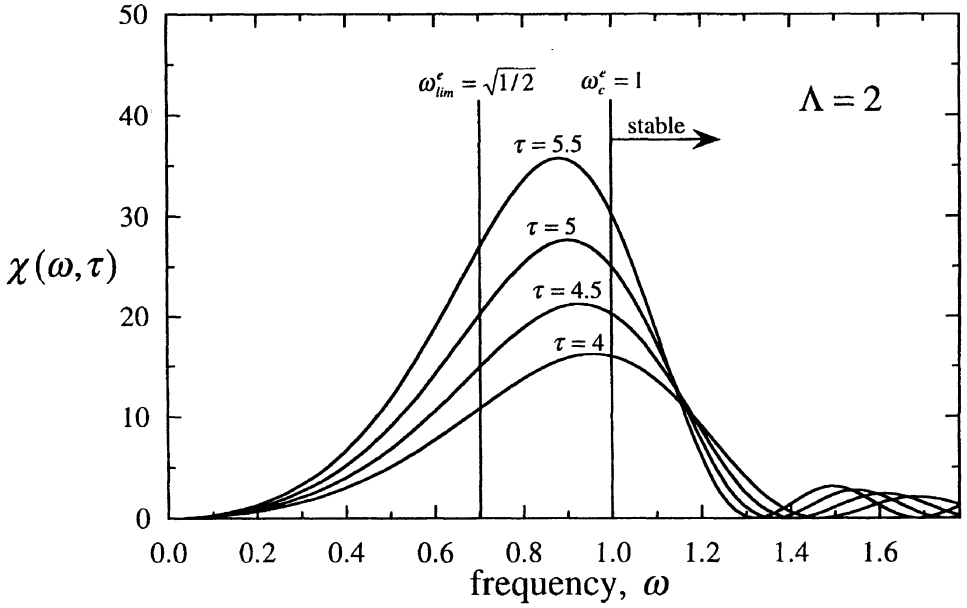

Fig. 6. The evolution in time of the amplification function versus initial imperfection frequency for a linear elastic constitutive relation.

blow up more rapidly than others. The frequency with the greatest rate of increase can be found by solving

$$\frac{\partial \chi}{\partial \omega} = 0, \tag{48}$$

where $\chi(\omega, \tau)$ is given by (44). Initially, at time $\tau = 0$, the frequency $\omega = \omega_c^e$ has the largest rate of increase, but as $\tau \to \infty$ this preferred frequency decreases towards

$$\omega_{\text{lim}}^e = \sqrt{\frac{\Lambda - 1}{2}}. \tag{49}$$

Although all imperfections with frequencies $\omega < \omega_c^e$ will grow exponentially, frequencies near the preferred frequency ω_{lim}^e will contribute to the most rapid failure.

3.2. *Ramberg–Osgood strain hardening*

So far the results obtained hold only for linear elastic materials. The more interesting and physically relevant solutions to the governing equation (24) are for nonlinear deformation. A representative nonlinear constitutive behavior is given by the Ramberg–Osgood strain hardening relation (25). An analytical solution to this nonlinear partial differential equation is unavailable. However, a finite difference method is found to give an accurate approximation to the solution. The time integration and the second order space derivative are approximated by a central difference method and the fourth order derivative is approximated by using a five node difference method. The nonlinear effective stress is obtained from (25) through the Newton method. The time step is controlled by the stability requirement. The details of the

numerical method are described in the Appendix. The input parameters are the applied load Λ, initial fiber displacement amplitude $\bar{\Upsilon}_m$ (or the initial imperfection angle $\bar{\psi}_m$) and the wavelength λ. The output is the fiber displacement distribution as a function of time $\Upsilon(\xi, \tau)$. The behavior of the displacement distribution as a function of time depends on the load level, and this will be used to find the critical load. The numerical method makes it possible to elucidate some characteristics of the dynamic plastic behavior of fiber composites under constant load, which are different from both the dynamic elastic behavior and static plastic microbuckling (Slaughter and Fleck, 1994).

3.2.1. *Deformation.* The solution to the nonlinear equation (24) is expressed in the form of (35). The amplification function χ has two dependent variables, time τ and position ξ. For the same given initial fiber waviness, different applied loads result in different amplification functions. Among all possible applied loads, the numerical results indicate that there exists a critical load Λ_c^d. If the applied load is greater than the critical load, the amplification function increases monotonically in time. This is analogous to the dynamic elastic critical load, and is called the dynamic plastic critical load. If the applied load is less than the dynamic plastic critical load, the amplification function is an oscillatory function of time. This solution is stable, and the fiber composite does not fail.

The numerical results indicate that when $\Lambda < \Lambda_c^d$, the fiber displacement distribution maintains a nearly sinusoidal profile. In other words, when the solution is stable the amplification function is a weak function of position; there is little localization of deformation. However, when $\Lambda > \Lambda_c^d$ there is a high degree of localization in the shear deformation. Representative elastic and plastic deformed fibers with initial wavelength $\lambda = 50$ and initial imperfection angle $\bar{\psi}_m = 4$ are plotted in Fig. 7. The applied load $\Lambda = 0.6$ is greater than the dynamic plastic critical load, as discussed below. The corresponding normalized effective shear strain distribution $\gamma_e/\gamma_y = \psi$ is plotted in

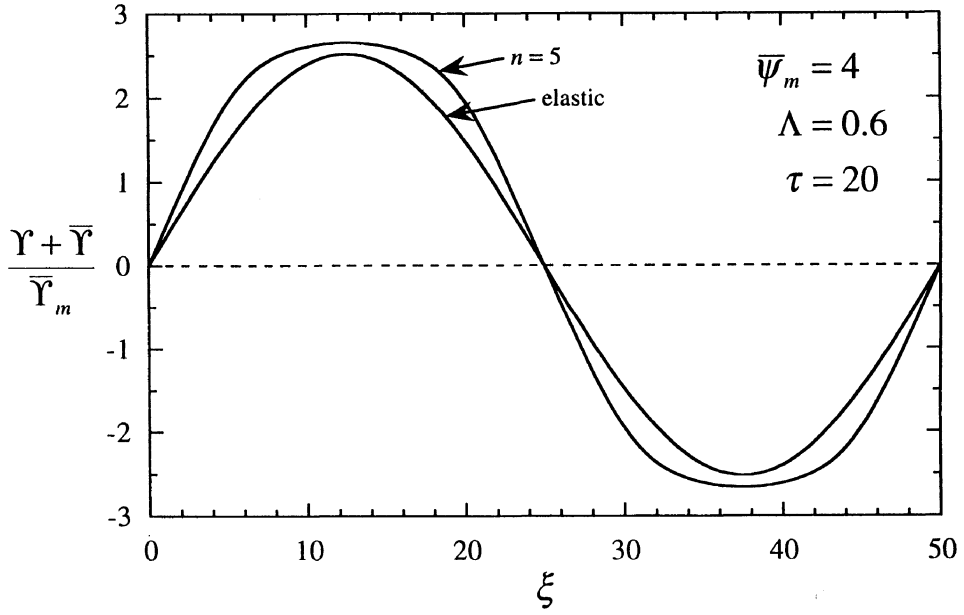

Fig. 7. The normalized deformed fiber profile of a composite with sinusoidal initial fiber waviness.

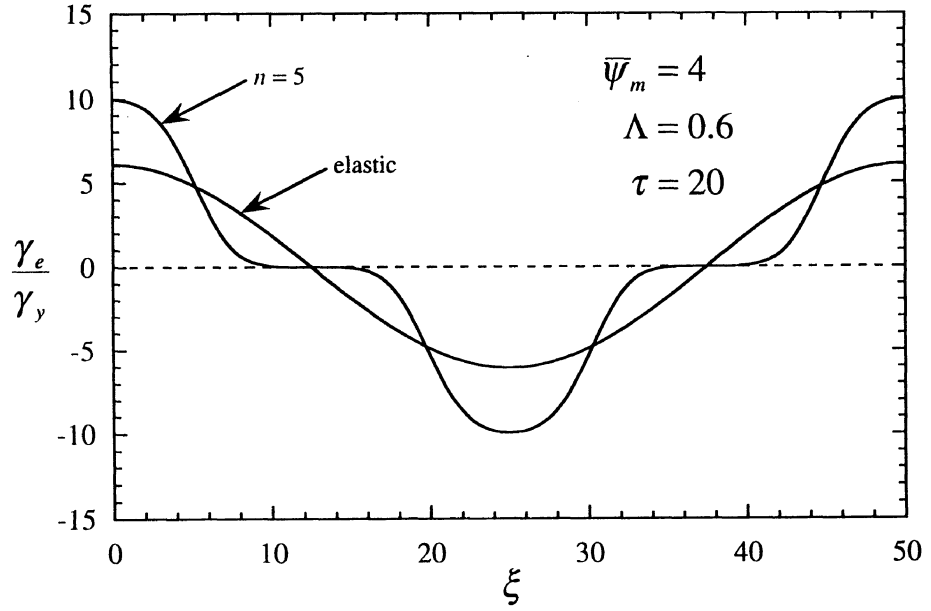

Fig. 8. Shear strain distribution in a deformed fiber composite. Shear localization occurs for a plastically deforming material.

Fig. 8. Figure 7 shows that the deformed configuration is no longer sinusoidal. Figure 8 illustrates the high degree of localization in deformation that occurs in regions of high initial fiber angle for the Ramberg–Osgood strain hardening material. This localization of deformation is interpreted as the formation of microbuckle kink bands. When $\Lambda > \Lambda_c^d$, the composite will be said to undergo dynamic plastic microbuckling.

3.2.2. *Critical load.* For a given frequency ω, there exists a dynamic plastic critical load Λ_c^d above which deformation will increase monotonically in time, and the fiber composite will fail. The procedure for obtaining this critical load is as follows. Because χ is a function of position as well as time, attention is paid to the maximum value χ_m which from symmetry occurs at the position $\xi = \lambda/4$;

$$\chi_m(\tau) = \chi\left(\frac{\lambda}{4}, \tau\right). \tag{50}$$

If $\Lambda > \Lambda_c^d$, the amplification function will increase monotonically with time, i.e.

$$\frac{\partial \chi_m}{\partial \tau} > 0. \tag{51}$$

This inequality will hold for all time. If $\Lambda < \Lambda_c^d$, the inequality

$$\frac{\partial \chi_m}{\partial \tau} < 0 \tag{52}$$

must hold at some point in the time history.

To find the critical buckling load Λ_c^d, begin with an initial guess of the load and check the derivative $\partial \chi_m/\partial \tau$. If $\partial \chi_m/\partial \tau > 0$ holds for all time (or some reasonably long

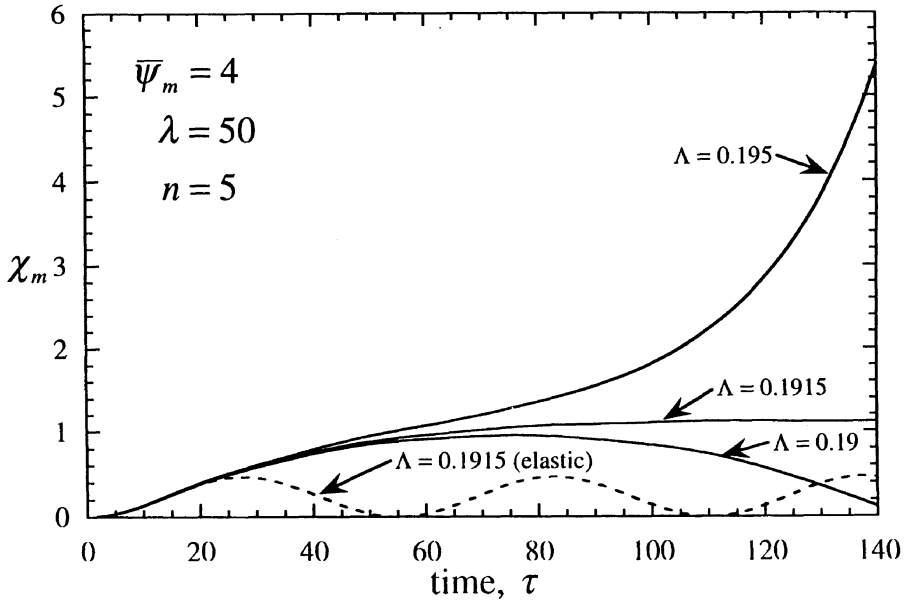

Fig. 9. The amplification function maximum versus time for different loads. For loads greater than the dynamic plastic critical load, the amplification increases monotonically with time. For loads less than the critical load, the amplification function oscillates.

period of time), reduce the load; if $\partial\chi_m/\partial\tau < 0$ holds during the time period, increase the load. Continue until the load at which

$$\lim_{\tau\to\infty} \frac{\partial\chi_m}{\partial\tau} \approx 0 \tag{53}$$

is found. This is the dynamic plastic critical load. An example of this procedure is shown in Fig. 9, where the initial imperfection angle $\bar{\psi}_m = 4$, the initial wavelength $\lambda = 50$, and the Ramberg–Osgood exponent $n = 5$. For the applied load $\Lambda = 0.195$, it is found that the amplification function increases monotonically; if the applied load is reduced to $\Lambda = 0.19$, the amplification function is bounded and oscillates in time; however, if the load is $\Lambda = 0.1915$, it is found that the solution neither blows up nor oscillates. This is the dynamic plastic critical load, $\Lambda_c^d = 0.1915$. The elastic solution for this load is shown for comparison in Fig. 9 as a dashed line. It is seen that the elastic solution is stable; the dynamic elastic critical load is greater than the dynamic plastic critical load, $\Lambda_c^e > \Lambda_c^d$.

Figure 10 shows the critical load as a function of the wavelength for different values of the Ramberg–Osgood parameter n and for the elastic solution. The initial imperfection angle is $\bar{\psi}_m = 4$. It is seen that for $\lambda > 20$ the critical load is nearly constant and that there is little dependence on n for $n > 5$. The dynamic plastic critical load is less than 25% of the dynamic elastic critical load for all Ramberg–Osgood exponents $n \geqslant 2$. The conclusion drawn is that the elastic solution for dynamic compressive failure of fiber composites greatly overestimates the critical load.

Figure 11 shows the critical load as a function of the initial imperfection angle for different values of the Ramberg–Osgood parameter n. The initial imperfection

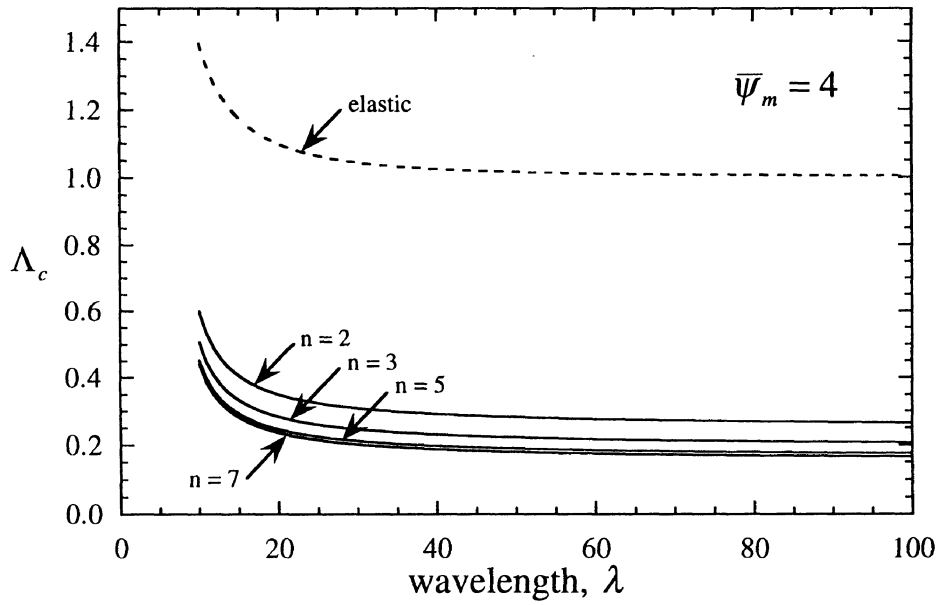

Fig. 10. The critical load versus initial imperfection wavelength for both elastic and plastic constitutive relations.

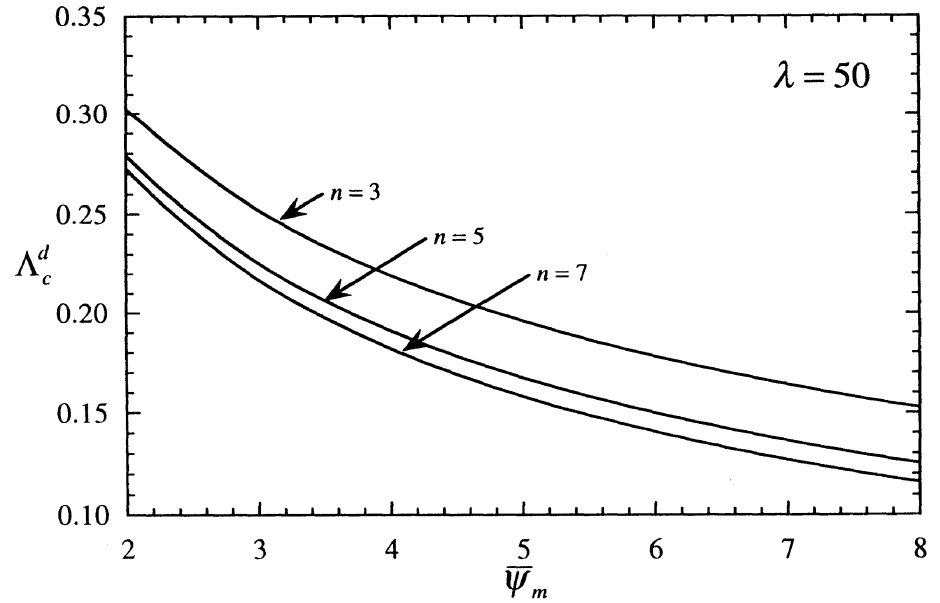

Fig. 11. The dynamic plastic critical load versus the initial imperfection angle.

wavelength is $\lambda = 50$. The dynamic plastic critical load decreases as the initial imperfection angle increases. It is seen again that there is little dependence on n for $n > 5$.

The dynamic plastic critical load is a function of initial wavelength, initial imperfection angle, and Ramberg–Osgood exponent

$$\Lambda_c^d = \Lambda_c^d(\lambda, \bar{\psi}_m, n). \tag{54}$$

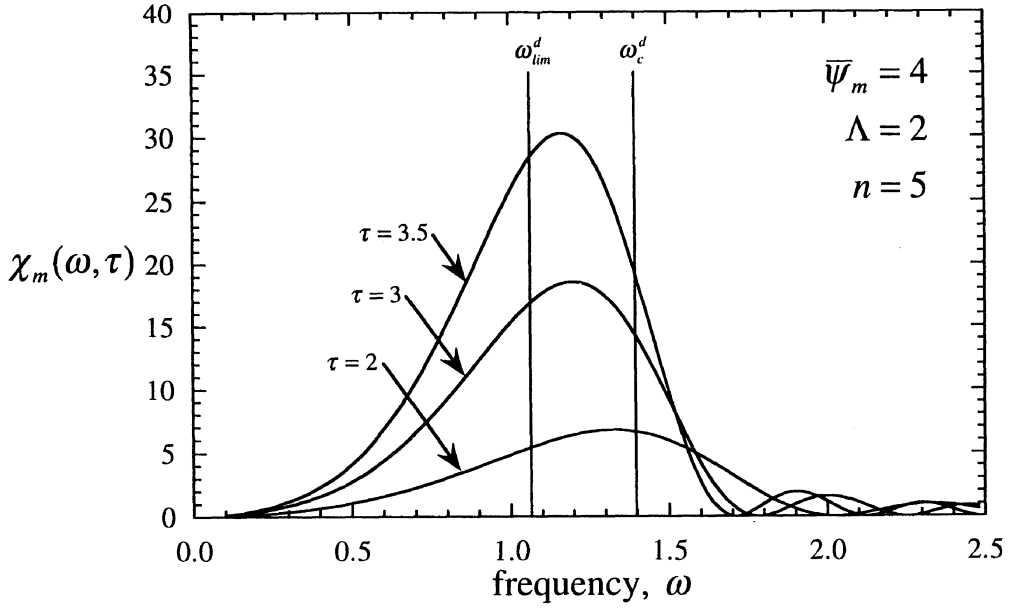

Fig. 12. The evolution in time of the amplification function versus initial imperfection frequency for a plastic constitutive relation.

This is in contrast to the dynamic elastic critical load, which is only related to the initial wavelength. For a typical polymer matrix fiber composite (T800/924C), $\lambda = 100, n = 4.5$ and $\bar{\psi}_m = 4$ (Soutis, 1991). In order to find an approximate analytical relation for (54) for engineering usage, the dependence of the critical load on λ and n is examined. The results indicate that (54) can be approximated by the following relation

$$\Lambda_c^d(\lambda, n) = a_0 + \frac{a_1}{(n-1)(\lambda-6)} + \frac{a_2}{n-1} + \frac{a_3}{\lambda-6}, \tag{55}$$

where $n > 1$, $\lambda > 6$ and $a_0, \ldots, a_s$ are parameters related to the initial imperfection angle $\bar{\psi}_m$. For $\bar{\psi}_m = 4$, a_0, a_1, a_2 and a_3 are 0.1340, 0.3000, 0.1178 and 1.091, respectively. If the applied load is less than a_0, the solution will remain stable regardless of the values of λ and n. The relation (55) is based on over 100 computational data points covering a range of parameter values $n = 2$–7 and $\lambda = 10$–100. The relation can be extrapolated to cover larger Ramberg–Osgood exponents and longer initial wavelengths.

3.2.3. *Critical frequency.* For a given load Λ, initial imperfections with frequencies less than the dynamic plastic critical frequency ω_c^d will lead to amplification functions which blow up in time. This is shown in a plot of $\chi_m(\omega, \tau)$ versus frequency ω for different values of time τ at a load $\Lambda = 2$ (Fig. 12). For $\bar{\psi}_m = 4$ and $n = 5$, it is found numerically that $\omega_c^d \approx 1.4$. This figure resembles that for the elastic solution (Fig. 6). It is seen in comparing these figures that $\omega_c^d > \omega_c^e$; for a given load, the results for plastic deformation predict a wider spectrum of frequencies that will result in composite failure.

The rate at which $\chi_m(\omega, \tau)$ increases for $\omega < \omega_c^d$ is not uniform; there is a preferred

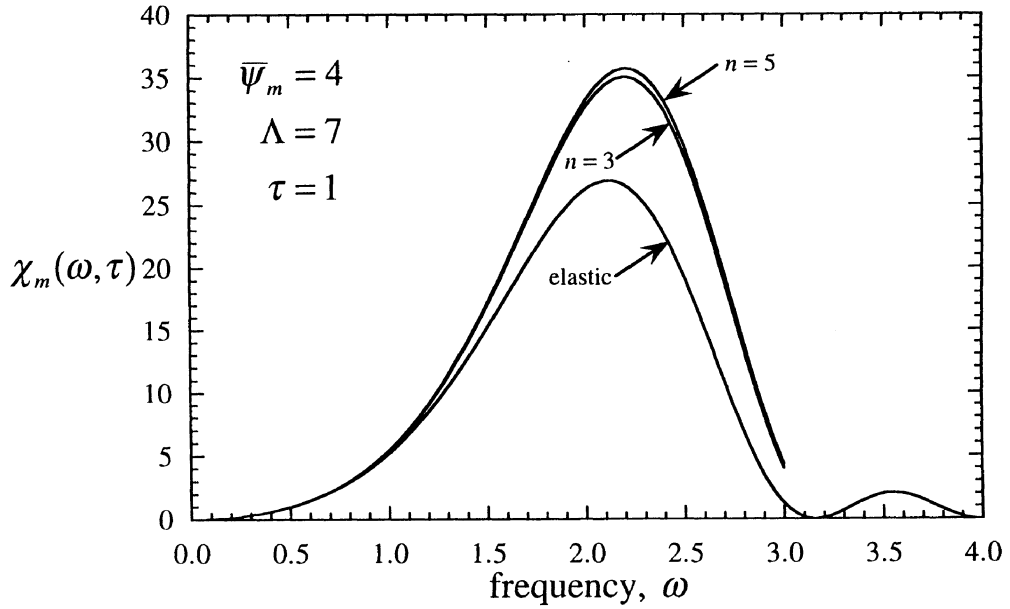

Fig. 13. The amplification function versus the initial imperfection frequency for a linear elastic constitutive relation and for a plastic constitutive relation.

frequency which blows up most rapidly. This preferred frequency varies with time, starting at ω_c^d at time $\tau = 0$ and decreasing to asymptotically approach a limiting value ω_{lim}^d as $\tau \to \infty$. In Fig. 12, the limiting frequency is found to be $\omega_{lim}^d \approx 1.05$. In comparison with the elastic solution (Fig. 6), it is seen that $\omega_{lim}^d > \omega_{lim}^e$. The results for $\Lambda = 7$ are shown in Fig. 13 for the elastic solution and plastic solution with $n = 3$ and $n = 5$. The difference in preferred frequency narrows as the load is increased.

3.2.4. *Comparison of static and dynamic compressive failure.* The dynamic plastic critical load is normalized by the kinking model prediction of microbuckling and compared with the results of the static couple stress model (Slaughter and Fleck, 1994). The results are plotted in Fig. 14. The dynamic critical load is less than the static critical load when the initial wavelength is large. The predictions of the dynamic and static couple stress models converge for small initial wavelengths. This indicates that the inertial effect has more influence on initial imperfections with long wavelengths. Under constant applied load, the inertia favors microbuckling, which will cause the dynamic critical load to be less than the static critical load. The dynamic critical load is approximately 90% of the static critical load for large initial imperfection wavelengths.

The kinking model, which neglects fiber bending stiffness, provides a conservative bound for the compressive strength of fiber composites when compared to the static couple stress model. The fiber bending stiffness increases the critical stress for microbuckling. This increase is greatest for short wavelength initial imperfections. In contrast, under a constant dynamic load, inertia tends to decrease the critical load, particularly for large wavelength initial imperfections. As a consequence, the kinking model of microbuckling overestimates the critical stress for constant dynamic loading. A conservative bound for these conditions is given instead by the fitting relation (55),

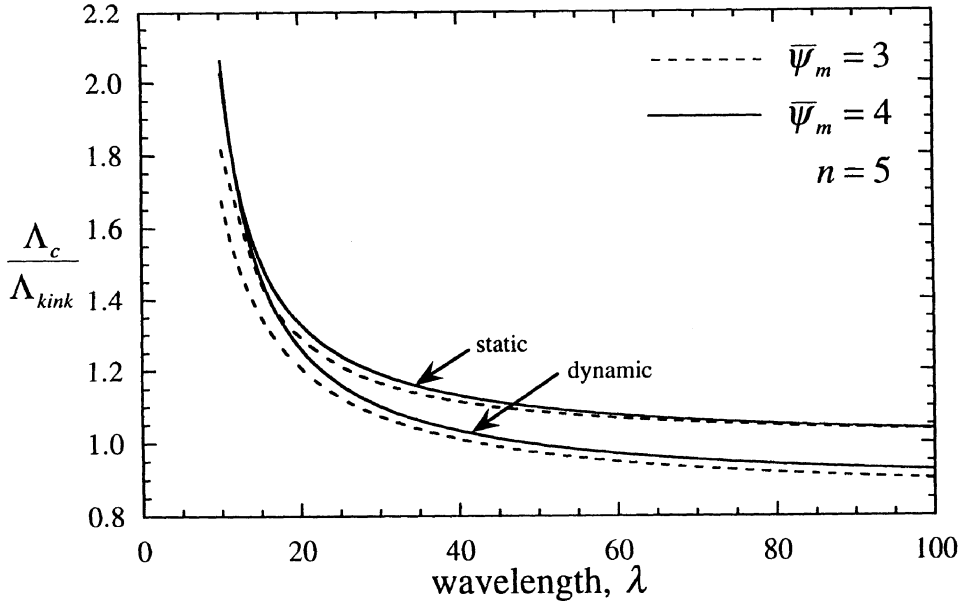

Fig. 14. Comparison between the dynamic critical load and the static critical load.

$\Lambda_c^d > a_0(\bar{\psi}_m)$. For $\bar{\psi}_m = 4$ (which corresponds to an initial imperfection angle of 2° for T300/924C), $a_0 = 0.1340$. For engineering purposes, the kinking analysis gives an acceptable estimate of the critical stress for initial imperfection wavelengths greater than 20 fiber diameters.

4. SUMMARY AND DISCUSSION

A dynamic coupled stress model has been presented for the axial compressive response of aligned fiber composites. The model accounts for fiber waviness and nonlinearity in the composite constitutive relations. The model was used to examine the response of fiber composites to a suddenly applied, constant compressive axial load. The initial waviness was assumed to be sinusoidal and both a linear elastic constitutive relation and a Ramberg–Osgood strain hardening constitutive relation were used. It was found that there is a critical load above which the composite is unstable, i.e. deformation of the composite increases monotonically with time. The unstable deformation is seen to localize spatially in regions of high initial fiber misalignment angle and this localization is interpreted as kink band formation, as is seen in static compressive microbuckling.

A comparison with the predictions for static microbuckling indicates that, for a constant load, the effects of inertia tend to decrease the critical load. Based on analysis of the static couple stress model, it has previously been stated (Slaughter and Fleck, 1994) that the analytical result of a kinking model given by Budiansky and Fleck (1993), which neglects the effect of fiber bending stiffness, provides a conservative bound to the critical compressive load for microbuckling. The analysis presented here

shows that this is not true if inertial effects are considered. Instead, a conservative bound is given by the numerically determined fitting parameter $a_0(\bar{\psi}_m)$ from (55).

For a given load, there is a range of fiber misalignment frequencies $0 < \omega \leqslant \omega_c$ (and wavelengths $2\pi/\omega_c \leqslant \lambda < \infty$), which will result in unstable deformation. Within this range, there is a preferred frequency for which deformation increases more rapidly than for the other frequencies. This preferred frequency varies with time, but tends asymptotically to a limiting value $\omega_{lim} < \omega_c$. The presence of a misalignment at this frequency will minimize the failure time of the composite.

A common apparatus used in the experimental study of the dynamic behavior of materials is the split Hopkinson pressure bar. This apparatus results in a state of constant axial strain rate, rather than constant load. A model for predicting the dynamic behavior of aligned fiber composites under constant strain rate is therefore of interest. An effort is currently underway to adapt the dynamic couple stress model to these load conditions. Ultimately, a model capable of analyzing general load or strain rate histories should be possible.

ACKNOWLEDGEMENT

Financial support from the ONR (grant 0014-91-j-1916) is gratefully acknowledged.

REFERENCES

Argon, A. S. (1972) Fracture of composites. *Treatise of Materials Science and Technology*, Vol. 1, pp. 79–114. Academic Press, New York.

Biot, M. A. (1967) Rheological stability with couple stresses and its application to geological folding. *Proc. R. Soc. A* **298,** 402–423.

Bogdanovich, A. and Friedrich, K. (1994) Initial and progressive failure analysis of laminated composite structures under dynamic loading. *Compos. Struct.* **27,** 439–456.

Budiansky, B. (1983) Micromechanics. *Comput. Struct.* **16,** 3–12.

Budiansky, B. and Fleck, N. A. (1993) Compressive failure of fiber composites. *J. Mech. Phys. Solids* **41,** 183–211.

Evans, A. G. and Adler, W. F. (1978) Kinking as a mode of structural degradation in carbon fiber composites. *Acta Metall.* **26,** 725–738.

Fleck, N. A. and Budiansky, B. (1990) Compressive failure of fiber composites due to micro-buckling. *Proceedings of the IUTAM Symposium on Inelastic Deformation of Composite Materials*, Troy, NY, 29 May–1 June, 1990 (ed. J. Dvorak), pp. 235–273. Springer-Verlag.

Fleck, N. A. and Shu, J. Y. (1995) Microbuckle initiation in fibre composites: a finite element study. *J. Mech. Phys. Solids* **43,** 1887–1918.

Fleck, N. A., Deng, L. and Budiansky, B. (1995) Prediction of kink width in compressed fiber composites. *J. Appl. Mech.* **62,** 329–337.

Gilat, R. and Aboudi, J. (1994). Dynamic buckling of metal matrix composite plates and shells under cylindrical bending. *Compos. Struct.* **28,** 459–469.

Greif, R. and Hebert, B. (1995) Experimental techniques for dynamic characterization of composite materials. *J. Engng Mater. Technol.* **117,** 94–100.

Huang, Y. H. and Wang, S. S. (1989) Compressive fatigue damage and associated property degradation of aluminum-matrix composites. *Proceedings of the 4th Japanese–U.S. Conference on Composite Materials*, Washington, DC, 27–29 June, 1988, pp. 606–632. Technomic.

Hull, D. (1981) *An Introduction to Composite Materials*. Cambridge University Press.
Jelf, P. M. (1993) Compressive failure of aligned fiber composites. Ph.D. thesis, Cambridge University Engineering Department.
Jelf, P. M. and Fleck, N. A. (1992) Compressive failure mechanisms in unidirectional composites. *J. Compos. Mater.* **26,** 2706–2726.
Jenq, S. T. and Sheu, S. L. (1993) High strain rate compressional behavior of stitched and unstitched composite laminates with radial constraint. *Compos. Struct.* **25,** 427–438.
Jones, N. (1989) *Structural Impact*. Cambridge University Press.
Lagace, P. A., Ryan, K. F. and Graves, M. J. (1994) Effect of damage on the impact response of composite laminates. *AIAA J.* **32,** 1328–1330.
Lesieutre, G. A. (1994) Modeling frequency-dependent longitudinal dynamic behavior of linear viscoelastic long fiber composites. *J. Compos. Mater.* **28,** 1770–1782.
Mamalis, A. G., Manolakos, D. E., Demosthenous, G. A. and Ioannidis, M. B. (1994) Axial collapse of thin-walled fibreglass composite tubular components at elevated strain rates. *Compos. Engng* **4,** 653–677.
Piggott, M. R. and Harris, B. (1980) Compression strength of carbon, glass, and kevlar-49 fibre reinforced polyester resins. *J. Mater. Sci.* **15,** 2523–2538.
Rosen, B. W. (1965) Mechanics of composite strengthening. *Fiber Composite Materials*, pp. 37–75. American Society of Metals Seminar, Metals Park, OH.
Saravanos, D. A. (1994) Integrated damping mechanics for thick composite laminates and plates. *J. Appl. Mech.* **61,** 375–383.
Schapery, R. A. (1993) Compressive strength and failure time based on local buckling in viscoelastic composites. *Appl. Mech. Rev.* **46,** S221–S228.
Schulte, K. and Minoshima, K. (1991) Mechanisms of fracture and failure in metal matrix composites. *12th Risø International Symposium on Materials Science: Metal Matrix Composites Processing, Microstructure, and Properties* (ed. N. Hansen), pp. 123–147.
Shaw, D., Shen, Y. L. and Tsai, P. (1993) Dynamic buckling of an imperfect composite circular cylindrical shell. *Comput. Struct.* **48,** 467–472.
Sierakowski, R. L., Nevill, Jr., G. E., Ross, C. A. and Jones, E. R. (1971) Dynamic compressive strength and failure of steel reinforced epoxy composites. *J. Compos. Mater.* **5,** 362–377.
Silling, S. A. and Taylor, P. A. (1994) The simulation of composite material response under dynamic compressive loading. *Modelling Simul. Mater. Sci. Engng* **2,** 689–699.
Slaughter, W. S. and Fleck, N. A. (1993a) Compressive fatigue of fiber composites. *J. Mech. Phys. Solids* **41,** 1265–1284.
Slaughter, W. S. and Fleck, N. A. (1993b) Viscoelastic microbuckling of fiber composites. *J. Appl. Mech.* **60,** 802–806.
Slaughter, W. S. and Fleck, N. A. (1994) Microbuckling of fiber composites with random initial fiber waviness. *J. Mech. Phys. Solids* **42,** 1743–1766.
Slaughter, W. S., Fleck, N. A. and Budiansky, B. (1993) Compressive failure of fiber composites: the roles of multiaxial loading and creep. *J. Engng Mater. Technol.* **115,** 308–313.
Soutis, C. (1991) Measurement of the static compressive strength of carbon-fibre/epoxy laminates. *Compos. Sci. Technol.* **42,** 373–392.

APPENDIX A: NUMERICAL METHOD

A procedure for numerically solving the governing equation of the dynamic couple stress model is outlined. Attention is focused on the Ramberg–Osgood strain hardening constitutive equation (25). Rewrite the governing equation (24) as

$$\frac{\partial^2 \Upsilon}{\partial \tau^2} = \frac{\partial s}{\partial \xi} - \frac{\partial^4 \Upsilon}{\partial \xi^4} - \Lambda \frac{\partial^2 \Upsilon}{\partial \xi^2} - g(\xi), \tag{A.1}$$

where

$$g(\xi) \equiv \Lambda \frac{\partial^2 \bar{\Upsilon}}{\partial \xi^2}. \tag{A.2}$$

This is a one-dimensional dynamic equation. A finite difference method is used to approximate both the time derivative and the space derivatives in the governing equation (A.1).

A.1. Finite difference approximation

Let $\Upsilon_i^k \equiv \Upsilon(\xi_i, \tau_k)$ where $\xi_i \equiv i(\Delta L)$ and $\tau_k \equiv k(\Delta t)$. The finite difference expressions for the derivatives are given by

$$\left[\frac{\partial^2 \Upsilon}{\partial \tau^2}\right]_i^k = \frac{\Upsilon_i^{k+1} - 2\Upsilon_i^k + \Upsilon_i^{k-1}}{(\Delta t)^2}, \tag{A.3}$$

$$\left[\frac{\partial \Upsilon}{\partial \xi}\right]_i^k = \frac{\Upsilon_{i+1}^k - \Upsilon_i^k}{\Delta L}, \tag{A.4}$$

$$\left[\frac{\partial^2 \Upsilon}{\partial \xi^2}\right]_i^k = \frac{\Upsilon_{i+1}^k - 2\Upsilon_i^k + \Upsilon_{i-1}^k}{(\Delta L)^2}, \tag{A.5}$$

$$\left[\frac{\partial^4 \Upsilon}{\partial \xi^4}\right]_i^k = \frac{\Upsilon_{i+2}^k - 4\Upsilon_{i+1}^k + 6\Upsilon_i^k - 4\Upsilon_{i-1}^k + \Upsilon_{i-2}^k}{(\Delta L)^4}. \tag{A.6}$$

For the finite difference expression for $\partial s/\partial \xi$ in (A.1), take the partial derivative of (25) with respect to ξ

$$\frac{\partial^2 \Upsilon}{\partial \xi^2} = \frac{\partial s}{\partial \xi}\left(1 + \frac{3n}{7} s^{n-1}\right). \tag{A.7}$$

Therefore

$$\left[\frac{\partial s}{\partial \xi}\right]_i^k = \frac{\left[\dfrac{\partial^2 \Upsilon}{\partial \xi^2}\right]_i^k}{1 + \dfrac{3n}{7} s^{n-1}}. \tag{A.8}$$

Here, s can be obtained from (25)

$$\left[\frac{\partial \Upsilon}{\partial \xi}\right]_i^k = s + \tfrac{3}{7} s^n \tag{A.9}$$

by using Newton's method. The numerical governing equation is

$$\Upsilon_i^{k+1} = 2\Upsilon_i^k - \Upsilon_i^{k-1} + (\Delta t)^2 B_i^k, \tag{A.10}$$

where

$$B_i^k = \left[\frac{\partial s}{\partial \xi}\right]_i^k - \left[\frac{\partial^4 \Upsilon}{\partial \xi^4}\right]_i^k - \Lambda \left[\frac{\partial^2 \Upsilon}{\partial \xi^2}\right]_i^k - g(\xi_i). \tag{A.11}$$

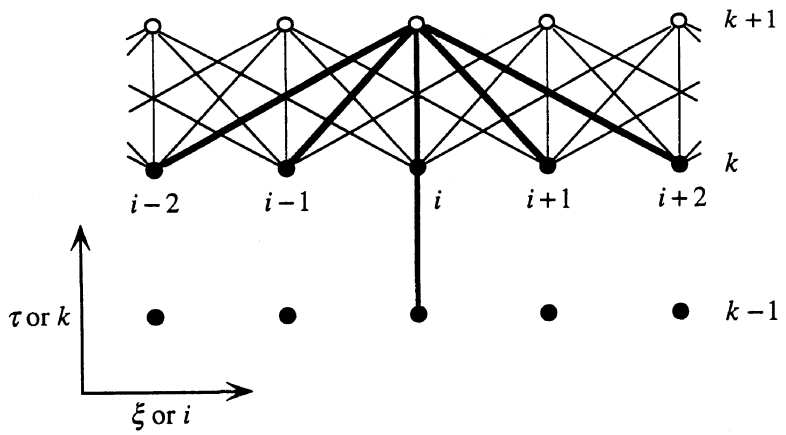

Fig. A1. Interdependence of nodes for stepping forward in time in the numerical procedure.

The computational procedure is shown in Fig. A1. Each unknown displacement is calculated based on six known displacements.

A.2. Time step

The time step is controlled by the stability requirement

$$\frac{(\Delta t)^2}{(\Delta L)^4} < 1, \tag{A.12}$$

which can be written as

$$\Delta t = c(\Delta L)^2, \tag{A.13}$$

where $c < 1$. In this paper $c = 0.2$.

A.3. Initial conditions

With the sinusoidal initial misalignment distribution

$$\bar{\Upsilon}(\xi) = \bar{\Upsilon}_m \sin\left(\frac{2\pi\xi}{\lambda}\right), \tag{A.14}$$

the function $g(\xi)$ is

$$g(\xi) = -\Lambda\left(\frac{2\pi}{\lambda}\right)^2 \bar{\Upsilon}_m \sin\left(\frac{2\pi\xi}{\lambda}\right). \tag{A.15}$$

The initial conditions are

$$\Upsilon_i^0 = 0,$$
$$\Upsilon_i^1 = -(\Delta t)^2 g(\xi_i). \tag{A.16}$$

A.4. Boundary conditions

For periodic sinusoidal initial waviness (A.14), the boundary conditions are given by

$$\Upsilon_0^k = 0,$$
$$\Upsilon_{(n)}^k = 0, \tag{A.17}$$

where $\lambda = n(\Delta L)$. The input parameters are the applied load Λ, the initial wavelength λ, the initial displacement amplitude $\bar{\Upsilon}_m$ and the Ramberg–Osgood exponent n. The output result is the displacement distribution $\Upsilon(\xi, \tau)$.